Published in final edited form as:
Nanomedicine. 2010 February ; 6(1): 127–136. doi:10.1016/j.nano.2009.06.004.

Porous-wall hollow glass microspheres as novel potential nanocarriers for biomedical applications

Shuyi Li, MD PhD[a,*], **Lynsa Nguyen**[b], **Hairong Xiong, MD**[a,c], **Meiyao Wang, PhD**[d], **Tom C.-C. Hu, PhD**[b], **Jin-Xiong She, PhD**[d], **Steven M. Serkiz, PhD**[e], **George G. Wicks, PhD**[e], and **William S. Dynan, PhD**[a]

[a]Institute of Molecular Medicine and Genetics, Medical College of Georgia, Augusta, GA 30912

[b]Small Animal Imaging, Department of Radiology, Medical College of Georgia, Augusta, GA 30912

[c]Institute of Medical Virology, Wuhan University, Hubei Province, China 430071

[d]Center for Biotechnology and Genomic Medicine, Medical College of Georgia, Augusta, GA 30912

[e]Savannah River National Laboratory, Aiken, South Carolina 29808

Abstract

Porous-wall hollow glass microspheres (PW-HGMs) are a novel form of glass material consisting of a 10 to 100 micron-diameter hollow central cavity surrounded by a 1 micron-thick silica shell. A tortuous network of nanometer-scale channels completely penetrates the shell. We show here that these channels promote size-dependent uptake and controlled release of biological molecules in the 3–8 nm range, including antibodies and a modified single-chain antibody variable fragment (scFv). In addition, a 6 nm (70 kDa) dextran can be used to gate the porous walls, facilitating controlled release of an internalized small interfering RNA. PW-HGMs remained in place after mouse intratumoral injection, suggesting a possible application for the delivery of anti-cancer drugs. The combination of a hollow central cavity that can carry soluble therapeutic agents with mesoporous walls for controlled release is a unique characteristic that distinguishes PW-HGMs from other glass materials for biomedical applications.

Keywords

Drug delivery; microsphere; silica; mesoporous; controlled release; single-chain antibody; scFv; siRNA

INTRODUCTION

Glass materials are biocompatible and can be used safely in applications requiring permanent implantation (reviewed in [1]). Hench and coworkers reported in 1971 that

[*]Corresponding author. Institute of Molecular Medicine and Genetics, Room CB-2803, Medical College of Georgia, 1120 15th Street, Augusta, GA 30912, Telephone: 706-721-1671, Fax 706-721-8752, sli@mcg.edu.

glasses in the system SiO_2-CaO-NaO-P_2O_5 form a strongly bonded interface with normal bone [2]. These bioactive glasses have proven useful in dental, orthopedic, and tissue engineering applications and have been implanted in more than one million patients [1]. More recent studies have focused on the creation of "third generation" glass materials defined by their ability to elicit a specific cellular response at the molecular level [3]. Bioactive glass materials, or composites of bioactive glass and polymers, have been tested as delivery systems for antibiotics and other antibacterial agents, anti-inflammatory drugs, fluoride ions, vascular endothelial growth factor, bone morphogenetic proteins, and nitric oxide [4–11]. Glass materials have also been developed as a therapeutic radiation delivery system [12–14]. One successful clinical application is delivery of ^{90}Yittrium-doped glass microspheres via a catheter in the hepatic artery, causing the material to lodge in the tumor capillary bed where it delivers a tumor-ablative dose of up to 100 Gy of ionizing radiation [15–18].

Currently, use of glass materials for delivery of therapeutic agents requires either bonding to organic polymers or the deposition of chemical substances directly into the glass matrix. Here we describe a more general approach for drug delivery using glass materials. It is based on novel porous-wall hollow glass microspheres (PW-HGMs). These are micron-scale glass "balloons" with an internal cavity bounded by a 1 μm-thick mesoporous wall [19]. The PW-HGMs were developed originally by the US Department of Energy for gas purifications and storage, including hydrogen storage, greenhouse gas sequestration, and nuclear non-proliferation applications [19]. PW-HGMs are generally fabricated in sizes ranging from 10 to 100 μm, which is on the same order as the solid glass beads used for radioembolization [13,14]. Unlike solid microspheres, however, they have a large internal solvent-accessible volume [19]. In addition, the walls are characterized by worm-like, interconnected channels in a silica-rich matrix [19]. Atoms and molecules can migrate into the PW-HGMs via the porous walls, and a subsequent change in state (e.g., precipitation) can retain them within the interior volume [19]. These unique materials have not previously been tested for compatibility with biological macromolecules.

We hypothesized that PW-HGMs might be useful as potential nanocarriers for controlled delivery of macromolecular therapeutics. We therefore tested their ability to interact with proteins, carbohydrates, and nucleic acids. We find that small dextrans, proteins, and nucleic acids (less than about 3 nm diameter) pass freely in and out of the interior cavity of the PW-HGMs in a rapid and reversible interaction, whereas some larger molecules (5–6 nm diameter) enter the interior cavity but also adhere strongly to the channel walls. One of these, a 70 kDa dextran, can be used to gate the channels, allowing retention and slow release of a short interfering RNA (siRNA). The results suggest that PW-HGMs may be useful as a controlled release delivery vehicle for antibodies, recombinant antibody derivatives, as well as small oligonucleotides.

Materials

Fabrication of PW-HGMs

The process and apparatus for producing PW-HGMs has been described, along with methodologies for loading or filling these materials [20–23], Briefly, feed for producing PW-HGMs was a 20–40 μm sodium borosilicate glass powder, and containing a sulfate blowing agent. The powder was fed into a hot zone produced by a controlled gas-air flame, which softens the glass to allow formation of spherical particles. The blowing agent becomes unstable as it is heated, producing a glass bubble that expands to produce hollow glass microspheres. The material was quenched, and a flotation process was used to retrieve the desired initial products. These were heat-treated to produce two phases in the thin outer walls, one rich in silica and the other in sodium and boron. The hollow microspheres were

treated with 4 M HCl, which preferentially leaches the sodium and boron-rich phase, leaving interconnected channels in the silica-rich phase. In some experiments (as noted in the Figure Legends), dry sieving was performed to enrich for <20 μm diameter PW-HGMs. SEM and other physical analyses were conducted at the Savannah River National Laboratory and at the Advanced Characterization Center at Clemson University.

Fluorescently-labeled dextrans, proteins, and nucleic acids

Fluorescein-labeled dextrans were obtained from Sigma-Aldrich (St. Louis, MO). Fluorescently-labeled DNA was prepared by annealing a 5'-Alex Fluor 546-labeled oligonucleotide (d(AGCAAAACCTCATACAGAAAATTCATTTACTAACGTCTGGAAAGACGACAAAACT), Invitrogen (Carlsbad, CA)) to its unlabeled complement. Cy 3-labeled GAPDH siRNA was from Applied Biosystems (Austin, TX). Alexa Fluor 488-labeled goat anti-rabbit IgG was obtained from Invitrogen. Other proteins were from High Molecular Weight and Low Molecular Weight Gel Filtration Calibration Kits (GE Healthcare Life Sciences, Buckinghamshire, UK). A maltose-binding protein fusion to scFv 18-2 [24] was expressed in *Escherichia coli*, purified as described[25] , and reacted with Traut's reagent and folate-N-succimydyl 3-(2-pyridyldithio)-propionate (Thermo Scientific/Pierce, Rockford IL). For protein labeling, a 100 μg/ml solution of fluorescein isothiocyanate (FITC) was prepared in DMSO. A separate solution of each protein was prepared in PBS, adjusted to pH 7.5 to 8.0 with Na_2CO_3. FITC was added at a 3:1 molar ratio and reacted at 37 °C for 30 min, and the labeled product was separated by gel filtration chromatography using Sephadex G-25 (Pre-packed Disposable Columns PD-10, Cat.#: 17-0851-01, GE Healthcare Life Sciences).

Dextran, protein, and nucleic acid loading

Dry PW-HGMs (2–3 mg) were suspended in 50–100 μl of PBS containing 200 μg/ml of dextran, 200 μg/ml protein, or 2 μM nucleic acid and incubated at room temperature for 5–10 min. An aliquot was transferred to a glass-bottom microwell dish (MatTek Corp., Ashland, MA) for direct observation. The remainder was collected by gentle centrifugation, washed with 0.5 ml of PBS or fetal bovine serum, and centrifuged again to remove excess dextran, nucleic acid, or protein. The pellet was resuspended in 50–100 μl of PBS or fetal bovine serum for imaging. For sequential incubation experiments, 2 μM DNA or siRNA were incubated with PW-HGMs for 5–10 min, FITC-Dextran (70 kDa, 200 μg/ml) was added and incubation was continued for another 5–10 min. Washing was performed as described. Microscopy was performed using a Zeiss LSM 510 laser scanning confocal microscope with a 40X or a 63X oil objective or an Applied Precision Deltavision microscope with a 20X or a 60X oil objective.

Intratumoral injection

PW-HGMs (3.3 mg) were incubated with fluorescein-labeled 70 kDa dextran (200 μg/ml) in 100 μl PBS. Just before use, PW-HGMs were washed twice with PBS and resuspended in 500 μL of PBS. To quantify signal from a known amount of PW-HGMs, aliquots were withdrawn from the center of a uniform suspension using a cut-off 200 μl pipette tip, and the volumes indicated in legend to Fig. 5 were transferred to the wells of a 1% agarose gel. PBS was added to each well to bring the final volume to 100 μl. Animal experiments were performed at the Medical College of Georgia according to an Institutional Animal Care and Use Committee-approved protocol. To prepare for PW-HGM injection, 10^7 cells of the HH human cutaneous T-Cell lymphoma line were injected into the flank of a 6–8 week old nude mouse, which was held until the tumor reached 200–300 mm^3 volume [26]. A 250 μl volume of prepared PW-HGMs was withdrawn from suspension using a 22-gauge needle syringe and injected intratumorally at a depth of approximately 5 mm. Care was taken to avoid any excess PW-HGMs on the surface of the tumor, and validated by the bright field

images of the animals. The mouse was anesthetized with a 1:1 mixture of medical air and oxygen containing 2% isoflurane and maintained at this level on a heated stage during the subsequent imaging session. Fluorescence images were collected using a Xenogen IVIS Imaging System equipped with 445–490 nm bandpass filter for excitation and a 515–575 nm bandpass filter for emissions. Images were acquired with a 1 s exposure, and LivingImage 2.60 Software was used to perform a fluorescent overlay, which allowed the subtraction of background to produce the final images.

Results

Characterization of PW-HGMs

Representative batches of PW-HGMs were characterized by pycnometer densitometry, mercury intrusion porosimetry, optical microscopy, and SEM. The densities of PW-HGMs were 1.5 to 2.0 g/ml, and diameters ranged from 10 to 100 μm, with a mean of about 50 μm. The ink-bottle shaped pores had diameters ranging from about 10 nm, at the narrowest point, to about 300 nm. A SEM image of the PW-HGMs shows the smooth outer surface (Fig. 1A). A higher magnification view shows the typical wall thickness of 1 μm and reveals the porosity in the outer shell (Fig. 1B). These pores, which connect the exterior space with the interior volume of the microspheres, are the distinguishing characteristic of PW-HGMs.

Determination of size exclusion limit

To determine the empirical size exclusion limit for hydrated molecules, PW-HGMs were incubated with fluorescein-labeled cross-linked carbohydrate polymers (dextrans) of known size distribution. The average molecular weight and Stoke's radius of each type of dextran is listed in Table 1. Confocal microscopy was used to monitor the presence of fluorescent dextran in the external space, interior cavity, and walls. Prior to washing to remove unbound dextran, the 150 kDa, 70 kDa, and 10 kDa dextrans were seen to equilibrate between the external space and interior volume (Fig. 2A). By contrast, the brightness of the 500 kDa dextran fluorescence was greater in the external space than in the interior, and the 2 MDa was excluded from the interior. The results are consistent with an interpretation that the porous walls behave as molecular sieves, with the larger dextrans showing progressively less ability to enter. Relatively little dextran fluorescence was detected within the porous walls, with the striking exception of the 70 kDa dextran, which accumulated to levels exceeding its concentration in solution. (Fig. 2A, "After wash."). To illustrate that the 70 kDa dextran is indeed concentrated in the microsphere walls we have also presented a series of images representing optical sections along the Z-axis of PW-HGMs following washing (Fig. 2B).

Interaction of PW-HGMs with proteins

We hypothesized that size-dependent interaction of PW-HGMs with macromolecules might make them useful as a controlled-release delivery vehicle for proteins. We prepared a set of test proteins by reacting well-characterized globular protein molecular weight markers with FITC. The fluorescently labeled products were incubated with PW-HGMs and the preparations were imaged by confocal microscopy before and after washing. All six of the tested proteins entered the interior volume initially (data not shown). The two largest proteins, immunoglobulin G (IgG) and conalbumin, were retained following washing (Fig 3A). The results were reminiscent of the 70 kDa dextran, with some protein apparently concentrated within the walls.

To characterize the PW-HGM-protein interaction further, we measured the rate of loss during an extended observation period. We collected images of single PW-HGMs at 2h intervals using a Deltavision microscope with point-visiting capability. The signal slowly disappeared with time (Fig. 3B). Quantitative analysis of the fluorescence density showed

that protein was lost with first-order kinetics for at least the first 10 h, with a half-life of 6–7 h. The image shown is representative of the median behavior in the population; some PW-HGMs had longer retention half-lives, whereas others lost fluorescence immediately upon washing, perhaps reflecting the presence of unseen defects in the wall structure (data not shown).

We also tested the interaction of PW-HGMs with a therapeutic antibody fragment that is under development in our laboratory as a tumor radiosensitization agent [24]. This single-chain antibody variable fragment (scFv) consists of the heavy and light chain variable portions of an IgG, joined by a flexible linker and expressed as a maltose binding protein (MBP) fusion in *E. coli*. The presence of MBP promotes stability in the intracellular environment [27] and results in a total molecular weight of 75 kDa, within the range that is retained by PW-HGMs (Fig. 3A). The scFv was tagged with FITC to allow visualization and with folic acid to promote binding to high-affinity cell surface folate receptor alpha (FRα) [28]. Like the similarly sized conalbumin, the FITC-folate-scFv derivative was taken up and retained by the PW-HGMs (Fig. 3C). The washed PW-HGMs were incubated with FRα-positive KB cells, and transfer of fluorescent protein to the cell surface receptors was evident (Fig. 3D). Together, the results suggest that PW-HGMs may be useful for *in vivo* delivery of therapeutic antibodies and recombinant antibody derivatives.

Interaction of PW-HGMs with nucleic acids

To further assess the controlled release properties of the PW-HGMs, we explored their interactions with nucleic acids. We incubated the PW-HGMs with an annealed 55-mer DNA, which behaved much like the smaller dextrans, freely entering and exiting the interior volume, with some retention within the porous walls after washing (Fig. 4A). We also tested an siRNA, composed of a pair of annealed 21-nt RNAs. SiRNAs are in widespread development as therapeutic agents, although efficient delivery methods are the limiting factor in many applications (reviewed in [29,30]). Like the DNA oligonucleotide, siRNA freely equilibrated between the exterior medium and the interior cavity (Fig. 4B).

Based on the idea that the 70 kDa dextran was about the same size as the minimum diameter of the pores, we investigated whether it could be used to “gate” them in order to control the uptake or release of nucleic acid cargo. We loaded the PW-HGMs with Cy3-labeled siRNA, then incubated with fluorescein-labeled 70 kDa dextran. Prior to washing, the RNA was seen inside the PW-HGMs, and the dextran was enriched within the walls (Fig. 4C). After washing, some PW-HGMs retained the siRNA (although it leached out of others) (Fig. 4C). We performed time-lapse studies of release of siRNA from individual PW-HGMs (Fig. 4D) The signal density for siRNA was bright initially and declined with time. This result suggests the possibility of using PW-HGMs as a controlled release delivery vehicle for siRNA.

Visualization of 70 kDa dextran-loaded PW-HGMs following intratumoral injection

The PW-HGMs are considerably larger than blood cells and are thus too large for systemic administration by an intravenous route. However, they are approximately the same diameter as the solid glass microspheres that have been used for tumor radioembolization. As a first step toward determining whether PW-HGMs could be used in a similar way, we examined the fate of intratumorally injected 70 kDa dextran-loaded microspheres in a mouse tumor model. We first determined the sensitivity and linearity of the imaging system by loading PW-HGMs with FITC-70 kDa dextran, transferring them into the wells of an agarose gel, and imaging them. Quantitative image analysis revealed a linear relationship between the amount of material loaded and the corresponding photon counts (Fig. 5A). We then injected 250 μl of the same PW-HGMs intratumorally into a xenografted mouse. The anesthetized

live mouse was imaged using the CCD camera system. The image shows clear localization at the site of injection (Fig. 5B). The results suggest that PW-HGMs are retained at the site of intratumoral injection, and thus could be used for localized delivery of anti-tumor antibodies or siRNA.

Discussion

We present here an initial characterization of PW-HGMs, a unique material distinguished by large, solvent-accessible interior volume and mesoporous walls. Molecular dimensions appear to be the most important factor in determining the type of interactions between macromolecules and PW-HGMs. The porous walls function as molecular sieves, admitting dextrans with a Stokes radius up to 8.5 nm, whereas dextrans with a larger radius were progressively excluded. The walls also admitted up to at least 5.5 nm, as well as short double-stranded RNA and DNA molecules, which have a helical diameter of 2–3 nm. Results are consistent with prior measurements indicating ink-bottle shaped pores with a minimum, or limiting, diameter of about 10 nm.

Although oligonucleotides and small proteins freely equilibrated between the inside and the outside of the PW-HGMs, larger proteins in the 70–150 kDa range behaved differently, being retained after washing and slowly released on a time scale of several hours. The FITC-70 kDa dextran also had an anomolously strong affinity for the interior of the mesoporous walls, whereas the smaller and larger dextrans did not. We hypothesize that binding to the walls is greatest when the particle size distribution and the pore size distribution of the PW-HGMs have maximum overlap, because this allows a large fraction of the surface area of the particles to be in contact with the wall material at any given time, thus maximizing the opportunity for surface interactions. Assuming that there is a range of particle sizes and pore sizes, maximum overlap should occur somewhat below the absolute size exclusion limit. The data suggest that this might indeed be the case (i.e. the 150 kDa dextran equilibrated between the exterior and the interior, presumably by passing through a subset of pores at the larger end of the size distribution, but did not noticeably concentrate within the walls), Additional work will be needed to understand the mechanism of retention in detail.

Based on its empirically-determined affinity for the walls, we tested the ability of the 70 kDa dextran to modulate the release of a small duplex RNA. The dextran-gated PW-HGMs retained the oligonucleotide over a period of minutes to hours, whereas untreated PW-HGMs showed no long-term retention. This demonstrated ability to use one macromolecule to gate the release of another extends the possible range of applications of PW-HGMs as nanocarriers in biomedical applications. The initial characterization of PW-HGMs reported here used model proteins and nucleic acids that are well characterized and, in most cases, commercially available as fluorescent conjugates. Although it appears that size is a principal determinant of potential for interaction with PW-HGMs, we have not systematically explored other variables, such as surface charge. Clearly, it will be desirable to address additional variables more systematically in the future.

One of the factors driving interest in biomedical applications of PW-HGMs is that glass materials have been used clinically for more than two decades. Based on this experience, it is well established that glass is safe and biocompatible in the context of tissue engineering [1,31]. Some research has also been performed to evaluate the use of biocompatible glass materials as drug delivery systems [1,3–11]. Such “third generation” materials have the potential to elicit a specific biological response in the host tissue [3]. Glass materials currently used in biomedical applications are solid, however, and drug delivery applications require either an organic copolymer or incorporation of materials (such as metal ions) within

the glass matrix. The PW-HGMs afford a potentially more general vehicle for delivery of a range of materials, including oligonucleotides and proteins.

At 10–100 μm, the diameter of PW-HGMs is, at minimum, several fold larger than erythrocytes (7–8 μm) or leukocytes (7–18 μm), which are the cells normally present in the bloodstream. Because of their size, PW-HGMs are apparently unable to pass through capillary beds. Although it might be possible to reduce the size of the PW-HGMs by adjusting conditions during fabrication, the unique advantage of thin walls and a large interior volume would be correspondingly diminished (i.e., more of the total volume would be occupied by the walls and less by payload space). There are, however a number of potential *in vivo* applications where inability to pass through the microvasculature is either not required, or could be turned to advantage. One of these is tumor embolization. Solid glass microspheres, doped with ^{90}Y, have shown promise for the treatment of liver cancer. In a recent clinical trial, where 137 patients underwent 225 administrations of microspheres, treatment was well tolerated with acceptable toxicities, and tumor response and median survival were promising relative to historical controls [32]. In contrast to the solid microspheres PW-HGMs offer the prospect of delivering a wider range of soluble drugs, including macromolecules, without the complications inherent in the use of radiopharmaceuticals. In particular, our preliminary characterization of PW-HGMs suggests that they are compatible with delivery of therapeutic RNAs, an area that has been the subject of intense recent investigation.

Other potential applications include the use of PW-HGMs as topical biological delivery vehicles to body cavities, for example in treatment of laryngeal, nasopharyngeal and oropharyngeal cancers. They could be used to deliver antiviral agents, including siRNA, for the treatment of cervical precancerous lesions, or antibacterial agents to the outer or middle ear, to surgical incisions, or to wounds. Glass implants are already widely used in regenerative medicine, and PW-HGMs might find use as implants bearing cytokines to control inflammation or growth factors to promote healing. Another possible application is as a controlled release vehicle for oral medications.

It is notable that none of the approaches described here has yet been optimized. The composition of the glass, flame temperature, residence time, and cooling rate can all be adjusted to produce PW-HGMs that are best suited for biomedical applications. None of these studies have yet been performed; work here used PW-HGMs that had been developed for other uses. The 70 kDa dextran is the only material tested so far as a gating agent, and other approaches are possible using polymers of different sizes and composition, and using chemical bonding (rather than surface adsorption) as a mechanism of retention. Further development of PW-HGM technology will enhance the potential of this material for diverse applications.

Acknowledgments

WSD and JXS received funding as Eminent Scholars of the Georgia Research Alliance. We thank Robert J. Lee (Ohio State University) for supplying folate-SPDP and Darren Baker for technical assistance with microscopy.

This work was supported by the Medical College of Georgia and by the NIH Nanomedicine Roadmap Initiative (EY018244)

References

1. Hench LL. The story of Bioglass. J Mater Sci Mater Med. 2006; 17:967–978. [PubMed: 17122907]
2. Hench LL, Splinter RJ, Allen WC, et al. Bonding mechanisms at the interface of ceramic prosthetic materials. J Biomed Mater Res. 1971; 6:117–141.

3. Hench LL, Polak JM. Third-generation biomedical materials. Science. 2002; 295:1014–1017. [PubMed: 11834817]
4. Ladron de Guevara-Fernandez S, Ragel CV, Vallet-Regi M. Bioactive glass-polymer materials for controlled release of ibuprofen. Biomaterials. 2003; 24:4037–4043. [PubMed: 12834599]
5. Domingues ZR, Cortes ME, Gomes TA, et al. Bioactive glass as a drug delivery system of tetracycline and tetracycline associated with beta-cyclodextrin. Biomaterials. 2004; 25:327–333. [PubMed: 14585720]
6. Bonner BC, Clarkson JE, Dobbyn L, et al. Slow-release fluoride devices for the control of dental decay. Cochrane Database Syst Rev. 2006:CD005101. [PubMed: 17054238]
7. Leach JK, Kaigler D, Wang Z, et al. Coating of VEGF-releasing scaffolds with bioactive glass for angiogenesis and bone regeneration. Biomaterials. 2006; 27:3249–3255. [PubMed: 16490250]
8. Bergeron E, Marquis ME, Chretien I, et al. Differentiation of preosteoblasts using a delivery system with BMPs and bioactive glass microspheres. J Mater Sci Mater Med. 2007; 18:255–263. [PubMed: 17323156]
9. Xia W, Chang J, Lin J, et al. The pH-controlled dual-drug release from mesoporous bioactive glass/polypeptide graft copolymer nanomicelle composites. Eur J Pharm Biopharm. 2008; 69:546–552. [PubMed: 18248801]
10. Balamurugan A, Balossier G, Laurent-Maquin D, et al. An in vitro biological and anti-bacterial study on a sol-gel derived silver-incorporated bioglass system. Dent Mater. 2008; 24:1343–1351. [PubMed: 18405962]
11. Friedman AJ, Han G, Navati MS, et al. Sustained release nitric oxide releasing nanoparticles: characterization of a novel delivery platform based on nitrite containing hydrogel/glass composites. Nitric Oxide. 2008; 19:12–20. [PubMed: 18457680]
12. Conzone SD, Hall MM, Day DE, et al. Biodegradable radiation delivery system utilizing glass microspheres and ethylenediaminetetraacetate chelation therapy. J Biomed Mater Res A. 2004; 70:256–264. [PubMed: 15227670]
13. Ibrahim SM, Lewandowski RJ, Sato KT, et al. Radioembolization for the treatment of unresectable hepatocellular carcinoma: a clinical review. World J Gastroenterol. 2008; 14:1664–1669. [PubMed: 18350597]
14. Salem R, Hunter RD. Yttrium-90 microspheres for the treatment of hepatocellular carcinoma: a review. Int J Radiat Oncol Biol Phys. 2006; 66:S83–S88. [PubMed: 16979447]
15. Andrews JC, Walker SC, Ackermann RJ, et al. Hepatic radioembolization with yttrium-90 containing glass microspheres: preliminary results and clinical follow-up. J Nucl Med. 1994; 35:1637–1644. [PubMed: 7931662]
16. Dancey JE, Shepherd FA, Paul K, et al. Treatment of nonresectable hepatocellular carcinoma with intrahepatic 90Y-microspheres. J Nucl Med. 2000; 41:1673–1681. [PubMed: 11037997]
17. Herba MJ, Illescas FF, Thirlwell MP, et al. Hepatic malignancies: improved treatment with intraarterial Y-90. Radiology. 1988; 169:311–314. [PubMed: 3174978]
18. Houle S, Yip TK, Shepherd FA, et al. Hepatocellular carcinoma: pilot trial of treatment with Y-90 microspheres. Radiology. 1989; 172:857–860. [PubMed: 2549567]
19. Wicks GG, Heung LK, Schumacher RF. Microspheres and Microworlds. Am Ceram Soc Bull. 2008; 87:23–28.
20. Schumacher, R. Apparatus to Enhance the Uniform Formation of Hollow Glass Microspheres. US patent application number. PCT/US2006/046167. 2006.
21. Schumacher, R.; Wicks, GG.; Heung, LK. Hollow Porous-Wall Glass Microspheres for Hydrogen Storage. US patent application number. 10/946,464. 2004.
22. Schumacher, R.; Wicks, GG.; Heung, LK., et al. Hollow Porous-Wall Glass Microspheres for and Composition and Process for Controlling Pore Size and Pore Volume. US patent application number. 12/315,544.
23. Schumacher, R.; Wicks, GG.; Leung, LK. Hollow Porous-Wall Glass Microspheres for Hydrogen Storage. US patent application number. 11/256,442. 2005.
24. Li S, Takeda Y, Wragg S, et al. Modification of the ionizing radiation response in living cells by an scFv against the DNA-dependent protein kinase. Nucleic Acids Res. 2003; 31:5848–5857. [PubMed: 14530433]

25. Xiong H, Li S, Yang Z, et al. E. coli expression of a soluble, active single-chain antibody variable fragment containing a nuclear localization signal. Protein Expr Purif. 2009; 66:172–180. [PubMed: 19281848]

26. Chen J, Fiskus W, Eaton K, et al. Cotreatment with BCL-2 antagonist sensitizes cutaneous T-cell lymphoma to lethal action of HDAC7-Nur77-based mechanism. Blood. 2009; 113:4038–4048. [PubMed: 19074726]

27. Shaki-Loewenstein S, Zfania R, Hyland S, et al. A universal strategy for stable intracellular antibodies. J Immunol Methods. 2005; 303:19–39. [PubMed: 16045924]

28. Zhao X, Li H, Lee RJ. Targeted drug delivery via folate receptors. Expert Opin Drug Deliv. 2008; 5:309–319. [PubMed: 18318652]

29. Kim D, Rossi J. RNAi mechanisms and applications. Biotechniques. 2008; 44:613–616. [PubMed: 18474035]

30. Juliano R, Alam MR, Dixit V, et al. Mechanisms and strategies for effective delivery of antisense and siRNA oligonucleotides. Nucleic Acids Res. 2008; 36:4158–4171. [PubMed: 18558618]

31. Stanley HR, Hall MB, Clark AE, et al. Using 45S5 bioglass cones as endosseous ridge maintenance implants to prevent alveolar ridge resorption: a 5-year evaluation. Int J Oral Maxillofac Implants. 1997; 12:95–105. [PubMed: 9048461]

32. Sato KT, Lewandowski RJ, Mulcahy MF, et al. Unresectable chemorefractory liver metastases: radioembolization with 90Y microspheres--safety, efficacy, and survival. Radiology. 2008; 247:507–515. [PubMed: 18349311]

33. Dong, L.; Hoffman, A.; Yan, Q. Dextran permeation through poly(N-isopropylacrylamide) hydrogels. In: Cooper, S.; Bamford, C.; Tsuruta, T., editors. Polymer Biomaterials in Solution, as Interfaces and as Solids. Utrecht: VSP BV; 1995. p. 1009-1020.

34. Fasman, G. CRC Practical Handbook of Biochemistry and Molecular Biology. Boca Raton, FL: CRC Press; 1989.

35. Berg, JM.; Tymoczko, JL.; Stryer, L. Biochemistry. New York: W.H. Freeman; 2002. Biochemistry; p. 746-750.

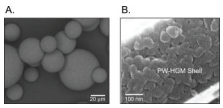

Figure 1.

Structure of porous-walled hollow glass microspheres (PW-HGMs)

A. Typical scanning electron micrographs of PW-HGMs. A. Whole microspheres. B. Cross section of mesoporous wall. Note presence of wormlike ~10 nm diameter channels.

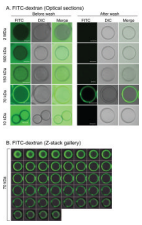

Figure 2.

Size exclusion limit determined using fluorescent dextrans. A. Confocal sections showing mixtures of PW-HGMs and fluorescein isothiocyanate (FITC)-labeled dextrans before and after washing with PBS to remove free dextran, as indicated. Panels show FITC, differential interference contrast (DIC) and merged images as indicated. Each panel is a single optical slice. Scale bars denote 10 μm. B. PW-HGMs were incubated with FITC-70 kDa dextran, then washed with PBS as in Panel A. Panel shows a series of images representing optical sections along the Z-axis for a single PW-HGM.

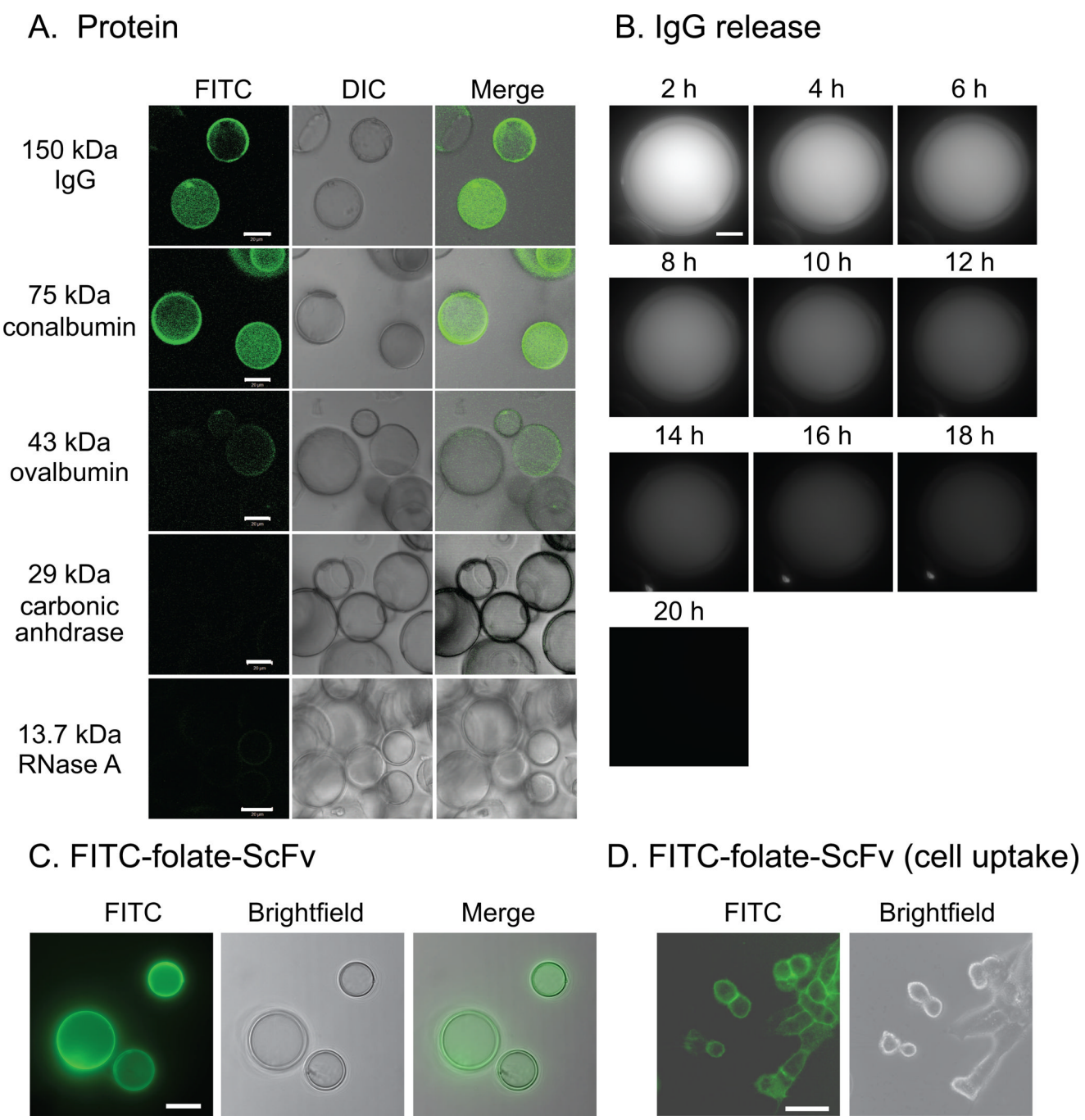

Figure 3.

Interaction of PW-HGMs with proteins. The indicated FITC-conjugated proteins were incubated individually with PW-HGMs as described in Materials and Methods. Molecular weights are provided for each protein (kDa). Confocal images were collected after washing with fetal bovine serum. Panels show FITC, DIC, and a merged image as indicated. B. Time course of IgG release. To allow for monitoring over a 20 h period, images were collected using an Applied Precision Deltavision deconvolution microscope with point visiting capability. Each panel shows a Z-stack projection. C. MBP-scFv fusion protein was derivatized with folate and FITC as described in Materials and Methods and incubated with PW-HGMs, which were washed with fetal bovine serum. Panels show FITC, brightfield and

deconvolution images. Each panel shows a single optical section. Scale bars denote 10 μm. D. Cell uptake. PW-HGMs were loaded with scFv as in Panel D, washed with fetal bovine serum, and allowed to incubate in contact with KB cells for 30 min at 37 °C. PW-HGMs were removed, and images were collected immediately. Each panel shows a single optical section. Scale bars denote 30 μm

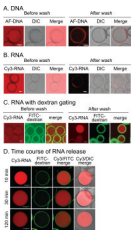

Figure 4.

Interaction of PW-HGMs with DNA and RNA oligonucleotides. A. 5'-Alex Fluor 546-labeled - DNA (55 base pair double stranded oligonucleotide) was incubated with PW-HGMs as described in Materials and Methods. Confocal images were collected before and after washing with PBS as in Fig. 2. B. Same, but with Cy3-RNA. C. RNA with dextran gating. PW-HGMs were incubated sequentially with Cy3-siRNA and FITC dextran. Images are shown before and after washing with PBS to remove free RNA and dextran. D. Time course of RNA release. PW-HGMs were incubated sequentially with Cy3-siRNA and FITC dextran, then washed in PBS and incubated for indicated times prior to imaging. All panels in this figure represent single optical sections. Scale bars denote 10 μm.

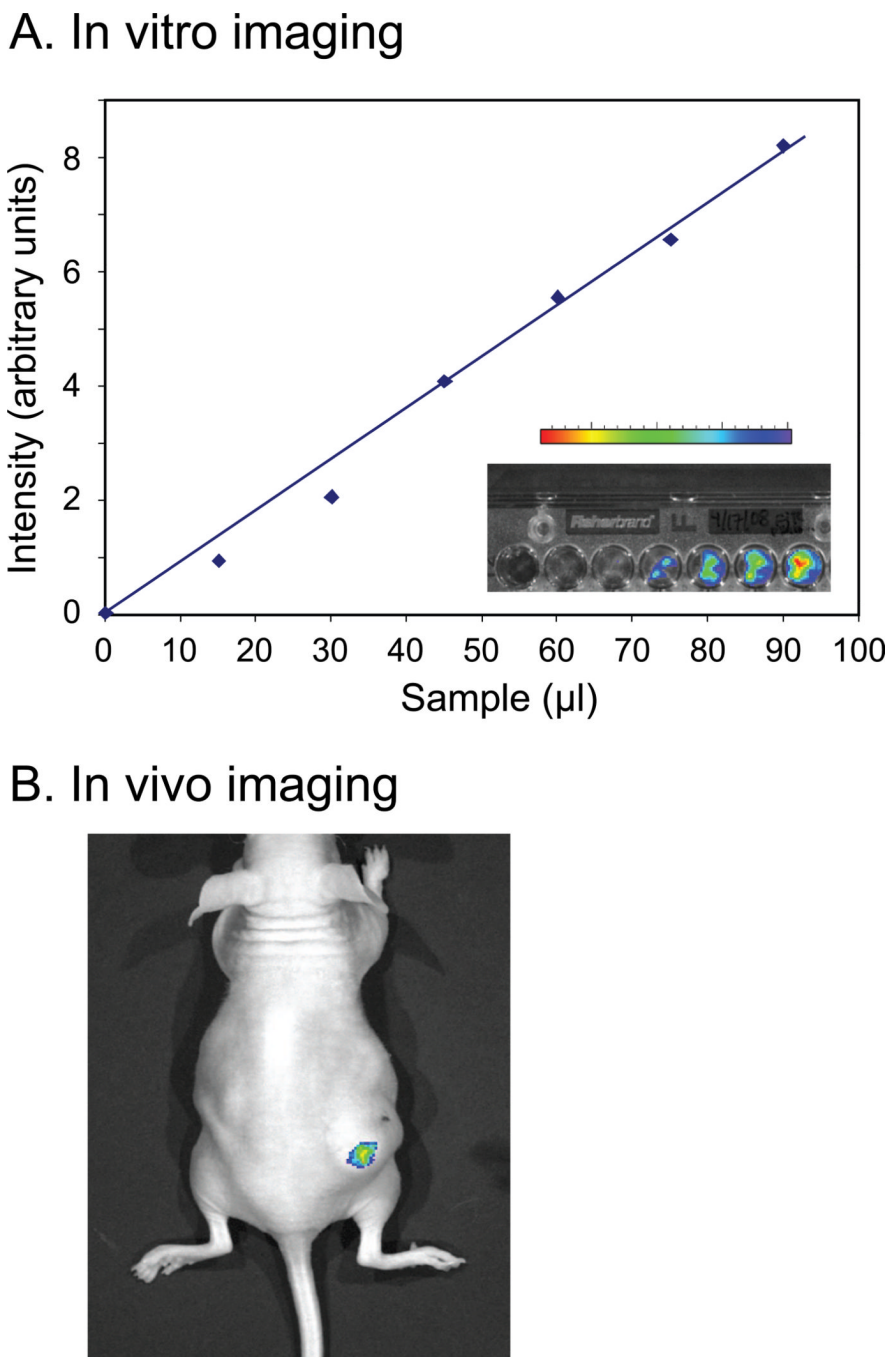

Figure 5.

Retention of FITC-dextran labeled PW-HGMs in a mouse tumor. A. Calibration curve. PW-HGMs were prepared by incubation with fluorescently-labeled 70 kDa dextran and imaged for green fluorescence as described in Materials and Methods. A. Calibration plot showing different amounts of PW-HGM preparation (0–90 µL). Photon counts are represented in arbitrary units. Inset shows gel image and associated false-color intensity bar. B. Image of mouse injected intratumorally with 250 µL of PW-HGM suspension.

Table 1

Interaction of dextrans, nucleic acids, and proteins with PW-HGMs

Material		Mass	Dimensions	Charge	Enter interior	Bind walls
Dextran		2 MDa	28.0 nm	neutral	No	−
		500 kDa	14.4 nm	neutral	No	−
		150 kDa	8.5 nm	neutral	Yes	−
		70 kDa	6.0 nm	neutral	Yes	+++
		10 kDa	2.3 nm	neutral	Yes	+
DNA	55 nt duplex	36.3 kDa	2.2 × 18 nm	acidic	Yes	++
RNA	21 nt duplex	13.9 kDa	2.6 × 4.8 nm	acidic	Yes	+
Protein	IgG	150 kDa	5.3 nm	varies, pI 5.0–7.5	Yes	+++
	Conalbumin	75 kDa	NA	acidic, pI 5.9	Yes	+++
	Ovalbumin	43 kDa	2.7 nm	acidic, pI 4.6	Yes	+
	Carbonic anhydrase	29 kDa	NA	acidic, pI 6.6	Yes	−
	RNase A	13.7 kDa	1.6 nm	basic, pI 8.9	Yes	−
	MBP-scFv	75 kDa	NA	neutral, pI 6.8	Yes	+++

Dimensions of dextrans are from ref [33] and proteins are from ref [34]. Dimensions of RNA and DNA are based on A-helix and B-helix parameters, respectively [35]. Estimates of size and charge do not take into account fluorophore conjugation. Binding to walls was estimated visually.